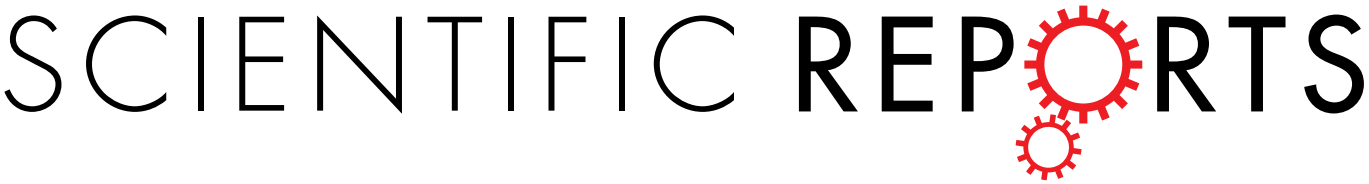

OPEN

Emergence of superconductivity in $(NH_3)_yM_xMoSe_2$ (M: Li, Na and K)

Xiao Miao[1], Saki Nishiyama[1], Lu Zheng[1], Hidenori Goto[1], Ritsuko Eguchi[1], Hiromi Ota[2], Takashi Kambe[3], Kensei Terashima[1], Takayoshi Yokoya[1,4], Huyen T. L. Nguyen[5], Tomoko Kagayama[5], Naohisa Hirao[6], Yasuo Ohishi[6], Hirofumi Ishii[7], Yen-Fa Liao[7] & Yoshihiro Kubozono[1,4]

Received: 02 November 2015
Accepted: 17 June 2016
Published: 11 July 2016

We report syntheses of new superconducting metal-doped $MoSe_2$ materials (M_xMoSe_2). The superconducting M_xMoSe_2 samples were prepared using a liquid NH_3 technique, and can be represented as '$(NH_3)_yM_xMoSe_2$'. The T_cs of these materials were approximately 5.0 K, independent of x and the specific metal atom. X-ray diffraction patterns of $(NH_3)_yNa_xMoSe_2$ were recorded using polycrystalline powders. An increase in lattice constant *c* showed that the Na atom was intercalated between $MoSe_2$ layers. The x-independence of c was observed in $(NH_3)_yNa_xMoSe_2$, indicating the formation of a stoichiometric compound in the entire x range, which is consistent with the x-independence of T_c. A metallic edge of the Fermi level was observed in the photoemission spectrum at 30 K, demonstrating its metallic character in the normal state. Doping of $MoSe_2$ with Li and K also yielded superconductivity. Thus, $MoSe_2$ is a promising material for designing new superconductors, as are other transition metal dichalcogenides.

Searching for new superconducting materials is one of the most challenging and exciting areas of research. During the past decade, iron pnictides (FeAs) and chalcogenides (FeSe) have attracted much attention, not only from researchers interested in developing new superconductors, but also physicists who are interested in the mechanism of superconductivity[1–4]. Recently, syntheses of metal-intercalated systems of FeSe using a liquid NH_3 technique have been extensively studied because various superconductors with high superconducting transition temperatures (T_cs) have been discovered[5–8]; the highest T_cs are 46 K at ambient pressure[5] and 49 K at high pressure[9]. The pressure-induced enhancement of T_c has also been confirmed for non-NH_3 K_xFeSe[10]. Thus a layered compound like FeSe is a promising material platform for investigating high-T_c superconductors.

The Mo dichalcogenide family has also attracted much attention because of the emergence of its unique physical properties[11,12] and potential use in high-speed transistors[13,14]. Electrostatic electron-doping of MoS_2 has produced superconductivity with a T_c as high as 10.8 K[11]. The plot of T_c versus the accumulated two-dimensional (2D) electron density n_{2D} showed a dome-shaped curve, *i.e.*, the T_c was tuned by the extent of electrostatic electron-doping. The maximum T_c was 10.8 K at 1.2×10^{14} cm^{-2}. Also, a signature of 2D superconductivity was observed in electrostatically electron-accumulated MoS_2[11]. The chemical doping of MoS_2 with alkali and alkaline-earth metal atoms[15,16] provided superconductivity with T_cs lower than the maximum T_c of electrostatically electron-accumulated MoS_2 [11,12]. The chemical doping of MoS_2 was achieved using the liquid NH_3 technique, and many superconducting materials have been produced.

Very recently, electron-doping of $MoSe_2$ was achieved by the electrostatic method[17], and the T_c was precisely tuned in the same manner as in MoS_2. In the case of $MoSe_2$, only a Sr atom was intercalated, and $MoSe_2$ then showed a T_c as high as 5.0 K[15]. This sample was prepared using the liquid NH_3 technique, and the chemical composition of Sr_xMoSe_2 can be expressed as '$(NH_3)_ySr_xMoSe_2$,' where the nominal x was 0.2. The shielding fraction of $(NH_3)_ySr_{0.2}MoSe_2$ was 60%.

Here, we report syntheses of M_xMoSe_2 samples (M: Li, K and Na) using the liquid NH_3 technique. In this study, Li, Na, K and Sr atoms were intercalated into $MoSe_2$ solids (only Sr-intercalation had previously been reported)[15].

[1]Research Laboratory for Surface Science, Okayama University, Okayama 700-8530, Japan. [2]Advanced Science Research Centre, Okayama University, Okayama 700-8530, Japan. [3]Department of Physics, Okayama University, Okayama 700-8530, Japan. [4]Research Centre of New Functional Materials for Energy Production, Storage and Transport, Okayama University, Okayama 700-8530, Japan. [5]Centre for Science and Technology under Extreme Conditions, Osaka University, Osaka 560-8531, Japan. [6]SPring-8/JASRI, Hyogo 679-5198, Japan. [7]National Synchrotron Radiation Research Center, Hsinchu 30076, Taiwan. Correspondence and requests for materials should be addressed to Y.K. (email: kubozono@cc.okayama-u.ac.jp)

Single-crystal-like agglomerations of $(NH_3)_yM_xMoSe_2$ (M: Li, Na, K and Sr) were produced. Na-intercalation in $(NH_3)_yNa_xMoSe_2$ was indicated by its synchrotron powder X-ray diffraction (XRD) pattern. Energy dispersive X-ray spectroscopy (EDX) showed its chemical composition, and the amount of NH_3 was also determined from the mass difference before and after reaction. The superconducting parameters were determined from the magnetic field (H) dependence of magnetization (M). The photoemission spectrum at 30 K showed a clear edge on the Fermi level, indicating metallic behavior in the normal state.

Results

Crystal structure of $(NH_3)_yNa_xMoSe_2$. Single crystals of pristine $MoSe_2$ were prepared using the annealing technique; details are described in the Methods section. A photograph of a pure $MoSe_2$ sample is shown in Figure S1a. A single-crystal structure analysis was produced using a piece of $MoSe_2$ (or single crystal) separated from a $MoSe_2$ agglomeration prepared in this study (Figure S1a); it is unclear whether an entire agglomeration is a single crystal or consists of multiple single crystals. A reasonable residual-factor (R) could be obtained in this analysis ($R = 2.4\%$ and weighted R (wR) $= 4.6\%$). Only one phase of $MoSe_2$ was included in the single crystal, and it was confirmed that no other phase such as Mo_3Se_4 was included. The structure of the $MoSe_2$ single crystal was hexagonal (space group: No. 194, $P6_3/mmc$). The lattice constants were $a = 3.289(7)$ Å and $c = 12.96(3)$ Å, which are consistent with those ($a = 3.283$ Å and $c = 12.918$ Å) reported previously for pristine $MoSe_2$[18]. Crystallographic data are listed in Table S1. As seen from the magnetic susceptibility M/H (emu $g^{-1} = cm^3 g^{-1}$) shown in Figure S2, no superconductivity was observed in any precursor $MoSe_2$ sample, implying no contamination with superconducting Mo_3Se_4. The chemical composition of one $MoSe_2$ agglomeration was determined to be '$MoSe_{1.9(2)}$' from the EDX spectrum (Figure S3). These analyses also show that the precursor material was not superconducting Mo_3Se_4[19], *i.e.*, it was non-superconducting $MoSe_2$. The EDX spectra, magnetic susceptibilities and single-crystal analyses guaranteed that all $MoSe_2$ agglomerations used for metal-intercalation throughout this study were in fact substantially '$MoSe_2$'.

Metal-doped $MoSe_2$ samples were prepared using the liquid NH_3 technique. The experimental details are described in the Methods section. Here, it is worth noting that instead of a polycrystalline powder, in this study, an agglomeration of $MoSe_2$ was used as the starting material for metal-intercalation. This is based on the successful synthesis of metal-doped FeSe from an agglomeration of FeSe[20].

A photograph of $(NH_3)_yNa_{0.5}MoSe_2$ prepared using the liquid NH_3 method is shown in Fig. 1a; the stoichiometry of Na ($x = 0.5$) is an experimental nominal value. The $(NH_3)_yNa_{0.5}MoSe_2$ samples (agglomerations) look like single crystals. The EDX spectrum for $(NH_3)_yNa_{0.5}MoSe_2$ is shown in Figure S4, which shows that the $(NH_3)_yNa_{0.5}MoSe_2$ sample is $(NH_3)_{0.4(1)}Na_{0.41(1)}MoSe_{2.04(1)}$. The amount of NH_3, $y = 0.4(1)$, was determined from the mass difference before and after the reaction that used liquid NH_3. These results indicate that NH_3 was included in this material, and the amount of Na is reasonably consistent with the experimental nominal value. Here, we must consider the exact chemical structure and appropriate representation of NH_3, *i.e.*, which form exists in the $MoSe_2$ solid? Does it exist as molecular NH_3, or does it take some other form such as a metal-coordinated amide? To determine the exact chemical formula, neutron diffraction may be required. Throughout this paper the simple chemical formula, $(NH_3)_yM_xMoSe_2$, is used for convenience because the exact chemical form of NH_3 is unclear.

The structure of $(NH_3)_yNa_{0.5}MoSe_2$ (0.5 is a nominal experimental value) was examined as a typical example using single-crystal XRD data collected at room temperature. As seen in Figure S1b, the XRD Bragg spots are quite diffuse, indicating a very disordered crystal. Because of the diffuse spots, a definitive structural analysis could not be performed.

To confirm whether the Na atom is located midway in the space between $MoSe_2$ layers, the powder XRD pattern of $(NH_3)_yNa_{0.5}MoSe_2$ was measured with synchrotron radiation ($\lambda = 0.4137(1)$ Å). The XRD pattern is shown in Fig. 1b together with the pattern calculated based on Le Bail fitting. The Le Bail fitting was performed for two phases under the space group of $P6_3/mmc$. The sample was prepared from Na and $MoSe_2$ using the liquid NH_3 technique, and ground up for the acquisition of a powder XRD pattern. The a and c of the main phase were determined to be 3.541(2) and 14.810(4) Å, respectively, while those of the minor phase were 3.2615(1) and 12.8133(5) Å. The minor phase can be assigned to pure $MoSe_2$, the lattice constants of which are consistent with the values ($a = 3.289(7)$ Å and $c = 12.96(3)$ Å) determined for pure $MoSe_2$ single crystal in this study. As seen from Fig. 1b, the peak-intensity of 002 peaks for non-doped (minor) and Na-doped $MoSe_2$ (major) observed at angles below $2\theta = 5°$ were virtually the same, indicating that the fractions were almost equivalent. No other phase (such as metal-doped Mo_3Se_4) was found, which is reasonable because the precursor material before metal-doping was demonstrated to be $MoSe_2$.

The c of 14.810 Å of the main phase is larger by 1.85 Å than that of pure $MoSe_2$ (12.96(3) Å), indicating that the Na is located in the space between $MoSe_2$ layers. The a value also increased to 3.541(2) Å from 3.289(7) Å, but the expansion ($\Delta a = 0.252$ Å) is too small to be attributed to the intercalation of Na into the $MoSe_2$ layer. As discussed later, the intercalation of Na at a 2a site, *i.e.*, the space between $MoSe_2$ layers, seems to be the most reasonable explanation of the observed changes. The R and weighted pattern R (wR_p) were 3.2 and 4.8% in the Le Bail fitting, respectively, which are reasonable values that confirm the Le Bail analysis. The structure suggested is shown in Fig. 1c; in this structure, NH_3 is not shown. A more precise crystal structure that includes NH_3 must be determined using high-quality $(NH_3)_yNa_{0.5}MoSe_2$ single crystals that yield sharp Bragg spots. This study is now in progress.

In this study, we tried to perform Rietveld refinement based on the model listed in Table S2 of Supplementary Information; the atomic coordinates listed in Table S2 were obtained by a structural analysis based on single-crystal X-ray data, but a reasonable R factor could not be obtained in the analysis because of the diffuse Bragg spots collected from the single crystal (Figure S1b). The complete Rietveld refinement could not be achieved using the above model, so it was not possible to determine the exact location of the Na atom. However,

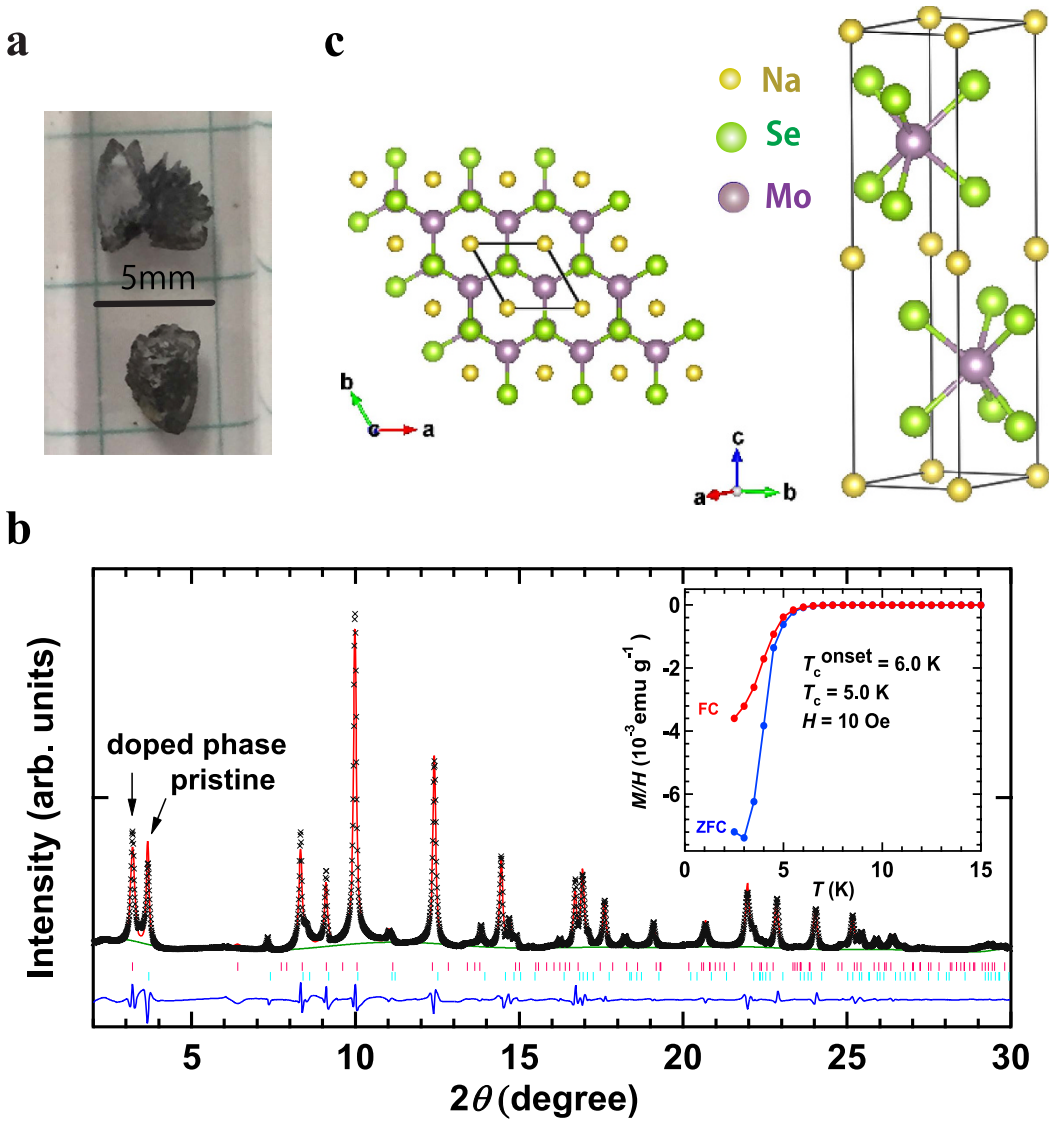

Figure 1. (**a**) Photograph of $(NH_3)_yNa_{0.5}MoSe_2$ agglomerations. (**b**) Powder XRD pattern of $(NH_3)_yNa_{0.5}MoSe_2$ using synchrotron radiation. 'x' marks correspond to the experimental XRD pattern. Red and green lines refer to calculated patterns (Le Bail fitting) and background, respectively. Ticks refer to the peak positions predicted. In (**b**), two phases ($(NH_3)_yNa_xMoSe_2$ and $MoSe_2$) are used in Le Bail fitting. The $M/H - T$ plots in ZFC and FC modes for the $(NH_3)_yNa_{0.5}MoSe_2$ sample providing the XRD pattern (**b**) are shown in the inset of (**b**). (**c**) Schematic representation of possible $(NH_3)_yNa_{0.5}MoSe_2$ structure; the structure was drawn based on the atomic coordinates shown in Table S2. As described in the text, this structure may be reasonable if the Na is located in the space between $MoSe_2$ layers, a possibility supported by the expansion of (**c**).

the large expansion of *c* suggests that Na is located in the space between $MoSe_2$ layers. If this is the case, the location of Na at a 2*a* site may be reasonable because of the presence of a large space around the 2*a* site. A possible crystal structure of $(NH_3)_yNa_xMoSe_2$ is shown in Fig. 1c.

Characterization of superconductivity in $(NH_3)_yNa_xMoSe_2$. Figure 2a shows the M/H – temperature (T) curves in zero field cooling (ZFC) and field-cooling (FC) modes for $(NH_3)_{0.4(1)}Na_{0.41(1)}MoSe_{2.04(1)}$. The T_c^{onset} and T_c were 6.0 and 5.0 K, respectively, for $(NH_3)_{0.4(1)}Na_{0.41(1)}MoSe_{2.04(1)}$; the T_c was determined from the crossing point of the extrapolation of the normal state and the drop of the $M/H - T$ curve in ZFC mode, as seen from the inset in Fig. 2a. Here, it may be necessary to briefly comment on a small slow decrease in M/H below T_c^{onset} (Fig. 2a). The inhomogeneous Na-doping of $MoSe_2$ may be suggested as its origin. However, as described later, the different x values in $(NH_3)_yNa_xMoSe_2$ did not provide different T_c or T_c^{onset} values, which means that the inhomogeneous Na-doping cannot explain the slow decrease. The second possibility is that the $(NH_3)_yNa_xMoSe_2$ agglomerations shown in Fig. 1a are not single crystals but aggregates of polycrystalline grains because the small size of superconducting grains often results in such a decrease. These possibilities are fully explored later.

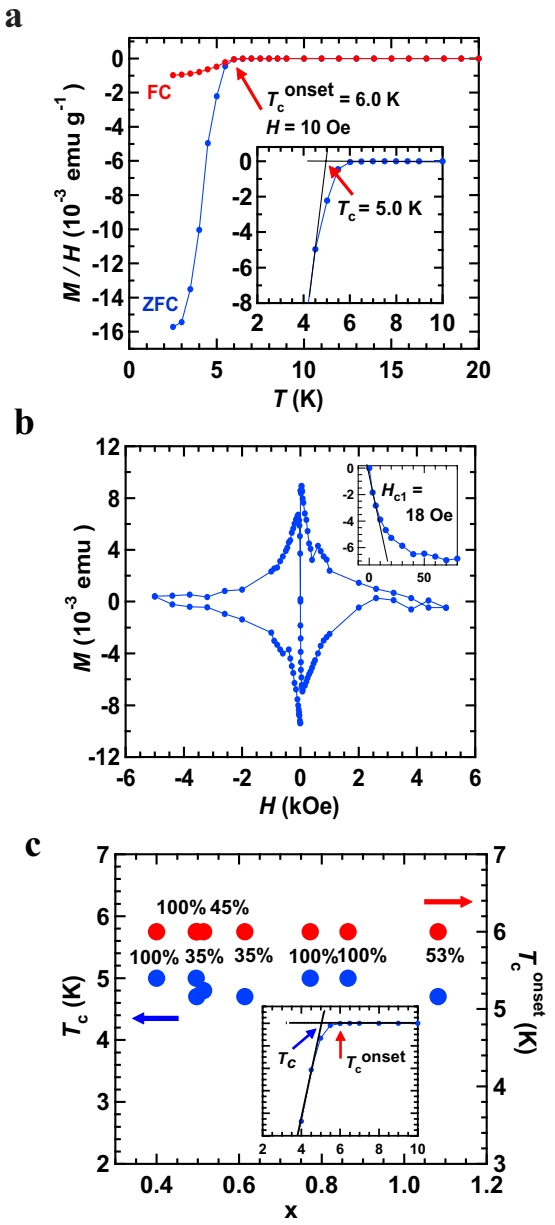

Figure 2. (**a**) *M*/*H vs. T* plots of the $(NH_3)_yNa_{0.5}MoSe_2$ agglomerations in ZFC and FC modes ($H = 10$ Oe). Inset in (**a**) shows the method used to determine T_c. (**b**) $M - H$ curve measured at 2 K for the $(NH_3)_yNa_{0.5}MoSe_2$ agglomerations. In the inset of (**b**), the expanded $M - H$ curve is shown together with the fitted line. The chemical composition of $(NH_3)_yNa_{0.5}MoSe_2$ used in (**a**,**b**) was determined to be $(NH_3)_{0.4(1)}Na_{0.41(1)}MoSe_{2.04(1)}$ (see text). (**c**) x-dependence of T_c and T_c^{onset} in $(NH_3)_yNa_xMoSe_2$; x was evaluated from the EDX. In (c) the shielding fraction is evaluated using the ρ determined using each chemical stoichiometry for $(NH_3)_yNa_xMoSe_2$; y is assumed to be 0.4. The inset of (**c**) shows how to determine the T_c and T_c^{onset}.

The shielding fraction at 2.5 K was 100% for $(NH_3)_{0.4(1)}Na_{0.41(1)}MoSe_{2.04(1)}$; the shielding fraction was evaluated using the density ($\rho = 5.64$ g cm^{-3}) determined from the above chemical stoichiometry and lattice constants shown in the previous section. Here it should be noted that the above sample was made by Na-doping of an agglomeration of $MoSe_2$. As a reference, the $M/H - T$ plot of the $(NH_3)_yNa_{0.5}MoSe_2$ sample prepared by Na-doping of polycrystalline $MoSe_2$ powder is shown in Figure S5 of Supplementary Information. The T_c and T_c^{onset} (Figure S5) were the same as those (Fig. 2a) of a sample prepared by Na-doping of a $MoSe_2$ agglomeration, but the shielding fraction was less than 1% at 2.5 K. The behavior of the $M/H - T$ plot below T_c^{onset} (Figure S5) was also the same as that shown in Fig. 2a. These results may show that effective Na-doping can be performed on these agglomerations of $MoSe_2$. Moreover, we suggest that the above small fraction (<1%) may originate in a limiting thickness of superconductivity, *i.e.*, a thin superconducting area formed by metal-doping using polycrystalline $MoSe_2$ powder. Therefore, throughout this paper, all studies were performed using the samples prepared by metal-doping of agglomerations of $MoSe_2$.

M	x (nominal value)	T_c (K)	T_c^{onset} (K)	r_{ion} (Å)
Na	0.3	5.0	6.0	1.02
Na	0.5	4.8	6.0	1.02
Na	0.5	5.0	6.0	1.02
Na	0.6	4.7	6.0	1.02
Na	0.6	4.7	6.0	1.02
Na	0.8	5.0	6.0	1.02
Na	0.8	5.0	6.0	1.02
Na	1.0	4.7	6.0	1.02
Li	0.5	5.0	6.5	0.76
K	0.5	5.3	7.5	1.38
Sr	0.2	5.0	7.0	1.18

Table 1. List of representative samples prepared in this study.

Finally, we comment briefly on the Meissner fraction of $(NH_3)_{0.4(1)}Na_{0.41(1)}MoSe_{2.04(1)}$ at 2.5 K (shielding fraction = 100% at 2.5 K (Fig. 2a)). The Meissner fraction was approximately 6.7% at 2.5 K which was evaluated from the $M/H - T$ plot in FC mode (Fig. 2a), indicating a small size for superconducting grains. Therefore, this single-crystal like $(NH_3)_{0.4(1)}Na_{0.41(1)}MoSe_{2.04(1)}$ may actually consist of polycrystalline superconducting grains, as previously suggested based on the slow drop observed in the $M/H - T$ plot below T_c^{onset} (Fig. 2a). However, some of $(NH_3)_yNa_xMoSe_2$ samples showed a Meissner fraction of more than 20%. Figure S6 shows $M/H - T$ plots of $(NH_3)_yNa_{0.5}MoSe_2$ exhibiting a Meissner fraction of 25%.

Figure 2b shows the $M - H$ curve at 2 K for $(NH_3)_{0.4(1)}Na_{0.41(1)}MoSe_{2.04(1)}$, which exhibits a clear diamond-like shape. The lower critical field H_{c1} was determined to be 18 Oe from the expanded $M - H$ curve (inset of Fig. 2b). It was concluded from the $M - H$ curve (Fig. 2b) that the upper critical field, H_{c2}, was > 0.3 T, indicating a type-II superconductor. Figure S7 shows $M/H - T$ plots at different H's, and the $H - T$ phase diagram (Figure S7) was constructed from the T_c^{onset} at each H; the fitted curve indicates the H_{c2} at each temperature. The positive curvature seen in Figure S7 is similar to the behavior of $(NH_3)_yK_xMoS_2$ reported recently[21]. The H_{c2} at 0 K, $H_{c2}(0)$, was evaluated to be 2.4 T. However, the data of the $H_{c2} - T_c$ plot are confined near T_c. Therefore, the H_{c2} is shown just for reference. We determined the London penetration depth, λ, to be 520 nm, from H_{c1}. The shape of the sample was assumed to be isotropic because the measurements of $M - H$ (2 K) and $M/H - T$ at different H's was performed using more than one agglomerations.

Figure 2c shows the x dependence of T_c in $(NH_3)_yNa_xMoSe_2$. The x value was determined from the EDX spectrum, and the x refers to the statistically averaged value with a small error bar falling within the range of the circle (Fig. 2c); the EDX was measured for several areas in one sample. The T_c was almost constant (~5 K) with an x-range of 0.4–1. The shielding fraction was higher than 35% in all samples. For the discussion, we plotted $T_c^{onset} - x$ in Fig. 2c again because the previous reports on metal-doped MoS_2 and $MoSe_2$ show the T_c^{onset}. The T_c^{onset} was also constant (~6 K) in the x-range of 0.4–1. Therefore, we cannot point to an x-dependence of superconductivity in $(NH_3)_yNa_xMoSe_2$. Finally, we must comment that the maximum x is 1.0 in $(NH_3)_yNa_xMoSe_2$ if the Na occupies only a 2*a* site in the $P6_3/mmc$ lattice, as described in the subsequent section. To sum up, it must be stressed that the x range must be 0–1 in $(NH_3)_yNa_xMoSe_2$. A list of typical superconducting samples is shown in Table 1.

Electronic structure of $(NH_3)_yNa_xMoSe_2$. The photoemission spectrum of a single-crystal-like agglomeration of $(NH_3)_yNa_{0.5}MoSe_2$ measured at 30 K is shown in Fig. 3a; the spectrum was recorded at the Γ point using the Xe-Iα resonance line (8.44 eV). The photoemission intensity was observed on the Fermi level, *i.e.*, the metallic edge was clearly recorded. This shows that $(NH_3)_yNa_{0.5}MoSe_2$ is metallic in the normal state, and the superconducting transition of $(NH_3)_yNa_{0.5}MoSe_2$ emerges from the metallic state. The evaluation of the superconducting gap in $(NH_3)_yNa_{0.5}MoSe_2$ has not yet been done due to the limited resolution of 15 meV in the photoelectron spectrometer, so this is future work. While the metallic edge was clearly observed in the normal state by Xe-Iα light, no signature of the metallic edge was obtained when changing Xe-Iα to the He-Iα resonance line (21.2 eV). We note that the surface of the $(NH_3)_yNa_xMoSe_2$ single crystal may be oxidized, as the photoemission spectrum using the Xe-Iα resonance line provides more bulk-sensitive results than He-Iα. The successful observation of the metallic edge at the Γ point is fully treated in the Discussion section.

Superconductivity in other metal-intercalated $MoSe_2$. Figure 3b,c show the $M/H - T$ curves for $(NH_3)_yLi_{0.5}MoSe_2$ and $(NH_3)_yK_{0.5}MoSe_2$, in ZFC and FC modes. The T_c^{onset} and T_c were 6.5 and 5.0 K, respectively, for $(NH_3)_yLi_{0.5}MoSe_2$, and were 7.5 and 5.3 K for $(NH_3)_yK_{0.5}MoSe_2$. The shielding fraction at 2.5 K was 21% for $(NH_3)_yLi_{0.5}MoSe_2$, and 10.5% for $(NH_3)_yK_{0.5}MoSe_2$. These shielding fractions were roughly estimated using the $\rho\,(= 6.99\ g\ cm^{-3})$ of $MoSe_2$ because the exact ρ could not be determined for $(NH_3)_yLi_{0.5}MoSe_2$ and $(NH_3)_yK_{0.5}MoSe$ owing to the absence of structural data (lattice constants). Therefore, the values may be slightly overestimated, but the shielding fraction suggests that the superconducting phases can be formed by intercalating alkali metal atoms other than Na. The T_c^{onset}s of these materials were higher than the 6 K of $(NH_3)_yNa_{0.5}MoSe_2$. However, the T_c was almost the same for three $(NH_3)_yM_xMoSe_2$'s. Furthermore, we synthesized the superconducting $(NH_3)_ySr_xMoSe_2$ (nominal x = 0.2), which showed a T_c (T_c^{onset}) as high as 4.8 K (7.0 K) ($M/H - T$ plots not

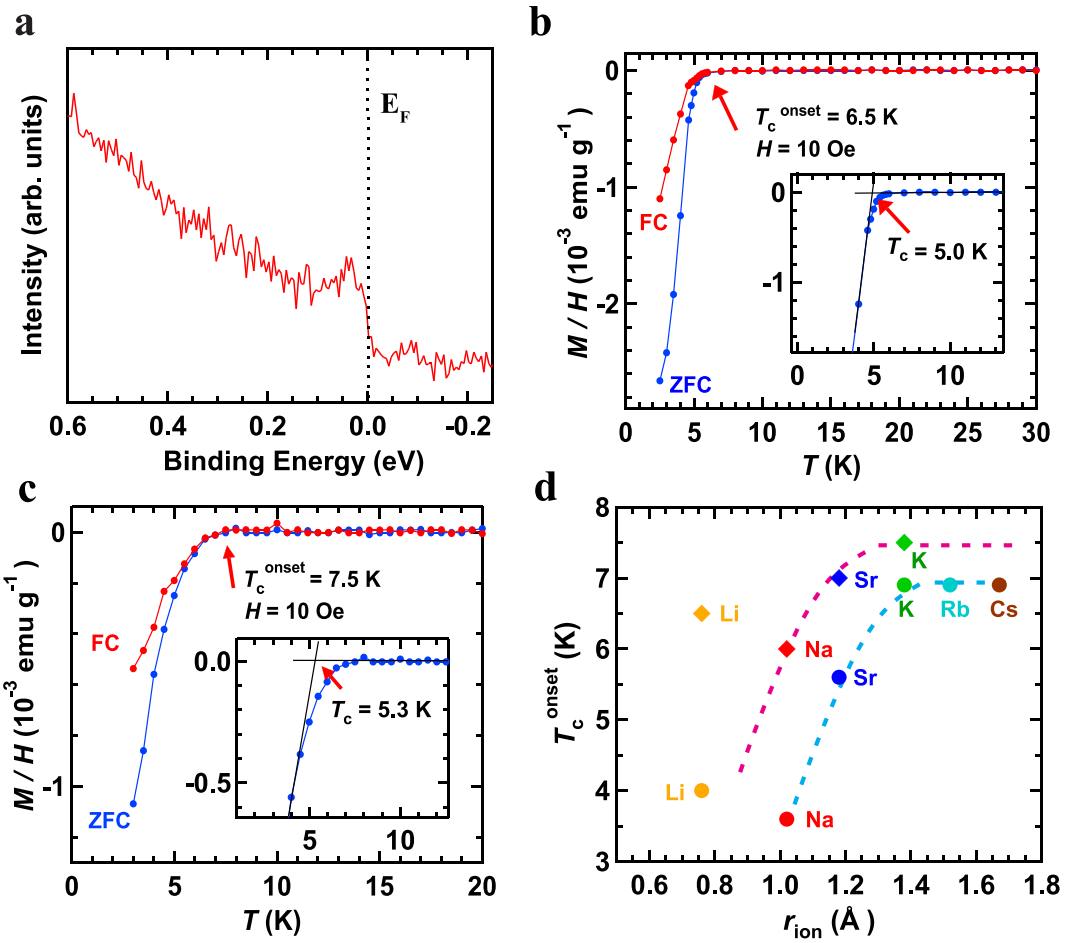

Figure 3. (**a**) Photoemission spectrum of $(NH_3)_yNa_{0.5}MoSe_2$. *M*/*H* versus *T* plots of (**b**) $(NH_3)_yLi_{0.5}MoSe_2$ and (**c**) $(NH_3)_yK_{0.5}MoSe_2$ agglomerations, respectively, in ZFC and FC modes ($H = 10$ Oe). (**d**) Plot of T_c^{onset} *vs.* r_{ion} in $(NH_3)_yM_xMoSe_2$ and $(NH_3)_yM_xMoS_2$. Circles and diamonds refer to $(NH_3)_yM_xMoS_2$ and $(NH_3)_yM_xMoSe_2$, respectively. The plot is based on the data collected in this study (diamonds) and those in Refs 15 and 16 (circles).

shown); the T_c was the same as that reported previously[15]. The shielding fraction was ~2.5% at 2.5 K which is lower than those of alkali-metal-doped $MoSe_2$.

In the case of $(NH_3)_yM_xMoS_2$, the T_c^{onset} generally increases with an increase in c[15], and it increases with the ionic radius (r_{ion}) of the intercalant. However, the T_c^{onset} of $(NH_3)_yLi_xMoS_2$ deviates from this pattern[15]. The T_c^{onset} vs. r_{ion} for $(NH_3)_yM_xMoSe_2$ (M: Li, Na, Sr and K) is plotted in Fig. 3d, together with that of $(NH_3)_yM_xMoS_2$ reported previously[15,16]. Similar behavior is seen in the plots of $T_c^{onset} - r_{ion}$ of $(NH_3)_yM_xMoSe_2$ and $(NH_3)_yM_xMoS_2$. The T_c^{onset} of $(NH_3)_yLi_xMoSe_2$ deviates from the suggested relationship, as does that of $(NH_3)_yLi_xMoS_2$ [15]. We briefly tried to synthesize $(NH_3)_yM_xMoSe_2$ (M: Rb, Cs, Ca, Ba, Sr and Yb) as well as $(NH_3)_yLi_{0.5}MoSe_2$, $(NH_3)_yNa_{0.5}MoSe_2$ and $(NH_3)_yK_{0.5}MoSe_2$. At the present stage, their superconductivity has not yet been observed, except for $(NH_3)_ySr_xMoSe_2$ which was previously reported[15].

Discussion

Very recently, Shi *et al.* succeeded in achieving superconductivity through electrostatic electron-doping of $MoSe_2$[17]. The maximum T_c of $MoSe_2$ reaches 7.1 K at $n_{2D} = 1.69 \times 10^{14}\,cm^{-2}$, and the T_c can be tuned by the accumulated electron density. The maximum T_c is lower than the 10.8 K of MoS_2[11] and the n_{2D} is higher than the $1.2 \times 10^{14}\,cm^{-2}$ of MoS_2[11]. For $MoSe_2$, a dome-like phase diagram of T_c vs. n_{2D} has not yet been observed because the number of metal-doped $MoSe_2$ superconductors discovered is still small, *i.e.*, a T_c in the n_{2D}-range ($>1.69 \times 10^{14}\,cm^{-2}$), which will be achieved by chemical electron-doping, has not yet been plotted.

A fresh $T_c - n_{2D}$ diagram (Fig. 4a) was prepared using the $T_c - n_{2D}$ plot (electrostatic electron-doping) reported by Shi *et al.*[17] and the $T_c - n_{2D}$ plot (chemical electron-doping) for $(NH_3)_yM_xMoSe_2$ samples produced in this study. Here, it should be noted that the 3D electron density, n_{3D}, evaluated from the x and lattice volume in $(NH_3)_yNa_xMoSe_2$ was translated to 2D electron density n_{2D} by assuming the thickness of the channel region to be one layer ($= c/2$); the electron concentration donated from a metal atom to the $MoSe_2$ layer was evaluated assuming that an alkali (alkali-earth) metal atom can donate only one (two) electron, *i.e.*, complex processes such as back-electron transfer to NH_3 were not considered. This is the same method used for the estimation of the $T_c - n_{2D}$ plot for metal-doped MoS_2[17]. In the phase diagram, the T_cs of $(NH_3)_yLi_{0.5}MoSe_2$, $(NH_3)_yK_{0.5}MoSe_2$ and $(NH_3)_ySr_{0.261(1)}MoSe_2$ are also plotted for reference, although the x is an experimental nominal value except

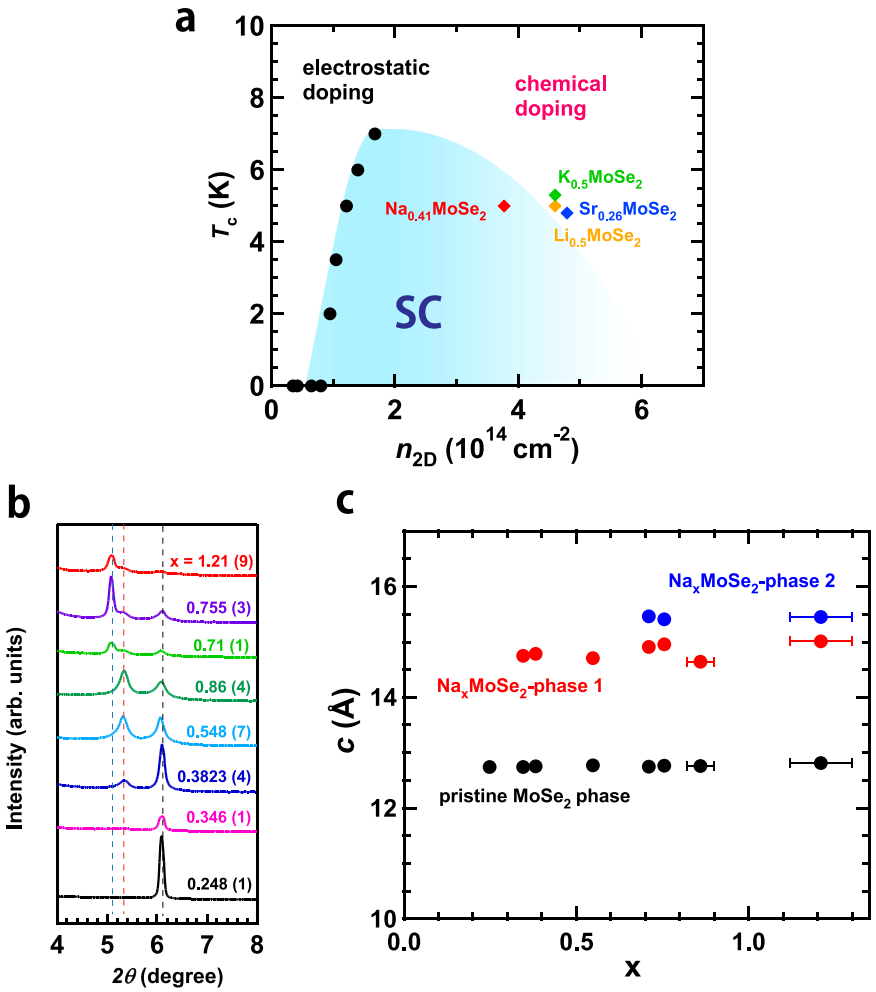

Figure 4. (**a**) Phase diagram of electron-accumulated $MoSe_2$. This phase diagram is based on the T_c^{onset} (diamonds) of $(NH_3)_yM_xMoSe_2$ (this work) and those (circles) of electrostatically electron-accumulated $MoSe_2$ recently reported by Shi *et al.*[17] '$(NH_3)_y$' is omitted in the formulas identifying differently M-intercalated $(NH_3)_yM_xMoSe_2$. (**b**) XRD patterns of $(NH_3)_yNa_xMoSe_2$ samples with different x; each x was determined from the EDX spectrum. The peaks at $2\theta = 6.1°$, 5.4° and 5.1° correspond to *002* peaks due to non-doped $MoSe_2$, $(NH_3)_yNa_xMoSe_2$ and another $(NH_3)_yNa_xMoSe_2$ phases, respectively. (**c**) x-dependence of *c* for the above three phases. The *c* values do not change with x.

in $(NH_3)_ySr_{0.261(1)}MoSe_2$. Consequently, a dome-like phase diagram was suggested in the same manner as MoS_2[11], but a continuous change of T_c was not obtained in the high n_{2D} range because of the almost identical T_c in metal-doped $MoSe_2$ prepared in this study (Fig. 4a).

As described in the Results section, the T_c^{onset} increases with increasing r_{ion} (Fig. 3d). This behavior is contrary to that of $(NH_3)_yM_xFeSe$, in which the T_c^{onset} is inversely proportional to the r_{ion}[7]. In the case of $(NH_3)_yM_xFeSe$, the T_c is closely associated with the FeSe plane spacing ($=c/2$)[7–9], and elements with a smaller r_{ion} produced larger FeSe plane spacings. This strange behavior can be explained by the fact that the crystal structure differs (off-center or on-center structures) depending on the r_{ion} of the intercalated element[8], so that $(NH_3)_yLi_xFeSe$, with an off-center structure, provides a larger FeSe plane spacing and high T_c (~44 K)[5,8]. If the T_c (or T_c^{onset}) also depends on the $MoSe_2$ plane spacing in $(NH_3)_yM_xMoSe_2$, the graph shown in Fig. 3d implies that an increase in the r_{ion} of the intercalant directly affects the $MoSe_2$ plane spacing. Actually, the deviation of T_c^{onset} of $(NH_3)_yLi_{0.5}MoSe_2$ and $(NH_3)_yLi_{0.5}MoS_2$ from the $T_c^{onset} - r_{ion}$ curve drawn in the graph shown in Fig. 3d may imply that $(NH_3)_yLi_xMoSe_2$ adopts a different structure from that (see Fig. 2c) determined for $(NH_3)_yNa_xMoSe_2$. In other words, we expect a different location for the Li atom in $(NH_3)_yLi_xMoSe_2$ than that of the Na atom (probably 2*a* site), as found in $(NH_3)_yLi_xFeSe$[6,8]. To sum up, we must discuss the superconductivity of $(NH_3)_yM_xMoSe_2$ in the light of two variables, n_{2D} and $MoSe_2$ plane spacing (or two dimensionality). This makes it difficult to observe a dome-like $T_c - n_{2D}$ phase diagram, as seen from Fig. 4a.

As described in the Results section (Fig. 2c), no x-dependence of T_c (or T_c^{onset}) was observed in $(NH_3)_yNa_xMoSe_2$. Here, it is very interesting and significant to investigate whether the lattice constants (*a*,*c*) change with the x value in $(NH_3)_yNa_xMoSe_2$. Figure 4b shows the expanded X-ray diffraction patterns ($2\theta = 4.0$–8.0°), indicating that the 002 peaks due to doped and non-doped phases are observed at the constant 2θ values

although the peak intensity due to the doped phase increases monotonically with increasing x in the x-range of 0.35 to 0.86. From this result, it was found that the *c* does not change with x, suggesting that the stoichiometric $(NH_3)_yNa_xMoSe_2$ is formed regardless of any increase in x. In other words, the chemical stoichiometry of $(NH_3)_yNa_xMoSe_2$ does not change even when x increases, and only the fraction of the non-doped phase decreases. Such behavior was recently observed in $(NH_3)_yK_xMoS_2$ [21], in which the $K_{0.4}MoS_2$ (2H structure) and $K_{1.0}MoS_2$ (1T and 1T' structure) are formed in low and high K concentrations, respectively. The constant T_c may be reasonably explained by the scenario that the stoichiometric $(NH_3)_yNa_xMoSe_2$ compound (or the chemical compound with fixed x and y) is formed in the entire x range, *i.e.*, the stoichiometric x value in $(NH_3)_yNa_xMoSe_2$ does not change with increasing x as determined from EDX; the EDX estimates the x value including non-intercalated Na atoms. This scenario corresponds to the third possibility described in the Results section.

As seen from Fig. 4b, at higher x values than 0.7, a new peak was observed, indicating the presence of a new *c*-expanded phase. Figure 4c shows the x-dependence of *c* in $(NH_3)_yNa_xMoSe_2$. From this graph, three different *c* values are found, due to (1) non-doped pure $MoSe_2$, (2) a Na-doped $MoSe_2$ phase, and (3) another Na-doped $MoSe_2$ phase with a larger $MoSe_2$ spacing. Since the T_c did not change in the entire x-range regardless of the formation of phase (3), it was unclear whether phase (3) is a new superconducting phase. To sum up, when x increases, two different Na-doped $MoSe_2$ phases with certain chemical stoichiometry seem to be formed in $(NH_3)_yNa_xMoSe_2$. Further study is necessary to clarify the exact stoichiometry of their phases.

Finally, it is necessary to comment on the observation of a metallic edge on the Fermi level in the photoelectron spectrum measured at the Γ point. The band dispersion in bulk crystals of pure $MoSe_2$ shows an indirect band gap (Γ – (ΓK))[22], where (ΓK) means an intermediate state between Γ and K. However, the band dispersion in a single layer of $MoSe_2$ shows a direct band gap (K – K)[22]. Therefore, a metallic edge for $(NH_3)_yNa_xMoSe_2$ should be observed at the (ΓK) point for $MoSe_2$ crystal if we assume a rigid-band picture of band dispersion. Furthermore, even if we assume a single-layer like $MoSe_2$ accompanied by expansion of the spacing between $MoSe_2$ layers due to Na-intercalation, a metallic edge must be observed at the K point. Therefore, a metallic edge should not be observed at the Γ point. Nevertheless, a metallic edge was clearly observed in the photoemission spectrum (Fig. 3a). Relevant to this question, it can be observed that the photoemission spectrum must detect all band dispersion of $(NH_3)_yNa_{0.5}MoSe_2$ since the single crystal of $MoSe_2$ must be disordered to possess different crystal alignments. In other words, the photoemission spectrum of a polycrystalline-like $(NH_3)_yM_xMoSe_2$ granule is recorded in Fig. 3a. This interpretation is reasonable since some disorder in the crystal is suggested by the XRD pattern shown in Figure S1b.

Methods

Sample preparation and characterization. Single crystals of $MoSe_2$ were formed from a polycrystalline powder $MoSe_2$ sample by physical vapor transport using a furnace with different temperature zones[23]; the powder $MoSe_2$ sample was prepared by annealing stoichiometric amounts of Mo and Se at 800 °C for 3 days and 1000 °C for 4 days, according to a procedure reported elsewhere[23]. To form single crystals of $MoSe_2$, $TeCl_4$ was mixed with a $MoSe_2$ sample as a transport material, the powder $MoSe_2$ sample was set in the 1000 °C source area, and $MoSe_2$ single crystals were collected in the low-temperature zone at 900 °C. Here we have used the term '$MoSe_2$ single crystal', but actually it is unclear whether the entirety of an agglomeration consists of one single crystal. Therefore, instead of the term 'single crystal', it may be valid to use the term 'agglomeration of $MoSe_2$.'

The samples of $(NH_3)_yM_xMoSe_2$ (M: Na, Li and K) were synthesized by the liquid NH_3 technique as follows: (1) stoichiometric amounts of $MoSe_2$ agglomerations and an alkali metal were placed in a glass tube, and then NH_3 gas was condensed in the tube. (2) The metal dissolved in the liquid NH_3 at −60 °C, and the solution (colored blue) was kept below −50 °C for 6 days. (3) When the color disappeared, the NH_3 was removed by dynamical pumping at room temperature. The same method was used for Sr-intercalation in $MoSe_2$.

The DC magnetic susceptibility (*M*/*H*) of all samples was measured using a SQUID magnetometer (Quantum Design MPMS2). The single-crystal XRD patterns of the samples were measured with a Rigaku Saturn 724 diffractometer with a Mo *K*α source (wavelength λ = 0.71078 Å). The powder XRD patterns of $(NH_3)_yNa_{0.5}MoSe_2$ and $(NH_3)_yNa_xMoSe_2$ (x = 0–1) were obtained using synchrotron radiation (λ = 0.4137(1) Å) from the BL10XU beamline and (λ = 0.6887 Å) from the BL12B2 beamline, respectively, of the Spring-8 in Japan; the incident beam was focused by a stacked compound X-ray refractive lens. The samples were introduced into quartz tubes in an Ar-filled glove box for *M*/*H* measurements, or into capillaries for XRD; the quartz tubes were pumped and sealed under vacuum, while the capillaries were sealed under Ar atmosphere. The EDX was obtained with an EDX spectrometer equipped with a scanning electron microscope (SEM) (KEYENCE VE-9800 - EDAX Genesis XM_2), and the photoemission spectrum with a SCIENTAOMICRON R4000 analyzer and a discharge lamp (SPECS). The Fermi level of the sample was referenced to that of gold, which was in electrical contact with the sample. The sample was cleaved in the ultrahigh-vacuum chamber for the measurement of photoemission spectrum. The photoemission spectrum was measured in an ultrahigh vacuum of $\sim 5 \times 10^{-9}$ Pa.

References

1. Kamihara, Y., Watanabe, T., Hirano, M. & Hosono, H. Iron-based layered superconductor $La[O_{1-x}F_x]FeAs$ (x = 0.05–0.12) with $T_c = 26$ K. *J. Am. Chem. Soc.* **130,** 3296–297 (2008).
2. Rotter, M., Tagel, M. & Johrendt D. Superconductivity at 38 K in the iron arsenide $(Ba_{1-x}K_x)Fe_2As_2$. *Phys. Rev. Lett.* **101,** 107006 (2008).
3. Hsu, F. C. *et al.* Superconductivity in the PbO-type structure a-FeSe. *PNAS* **105,** 14262–14264 (2008).
4. Chen, X. H. *et al.* Superconductivity at 43 K in $SmFeAsO_{1-x}F_x$. *Nature* **453,** 761–762 (2008).
5. Ying, T. P. *et al.* Observation of superconductivity at 30~46 K in $A_xFe_2Se_2$ (A = Li, Na, Ba, Sr, Ca, Yb, and Eu). *Sci. Rep.* **2,** 426 (2012).
6. Burrard Lucas, M. *et al.* Enhancement of the superconducting transition temperature of FeSe by intercalation of a molecular spacer layer. *Nat. Mater.* **12,** 15–19 (2013).
7. Zheng, L. *et al.* Superconductivity in $(NH_3)_yCs_{0.4}FeSe$. *Phys. Rev. B* **88,** 094521 (2013).

8. Zheng, L. *et al.* Emergence of multiple superconducting phases in $(NH_3)_yM_xFeSe$ (M: Na and Li). *Sci. Rep*. **5,** 12774 (2015).
9. Izumi, M. *et al.* Emergence of double-dome superconductivity in ammoniated metal-doped FeSe. *Sci. Rep*. **5,** 9477 (2015).
10. Sun, L. L. *et al.* Re-emerging superconductivity at 48 kelvin in iron chalcogenides. *Nature* **483,** 67–69 (2012).
11. Ye, J. T. *et al.* Superconducting dome in a gate-tuned band insulator. *Science* **338,** 1193–1196 (2012).
12. Taniguchi, K., Matsumoto, A., Shimotani, H. & Takagi, H. Electric-field-induced superconductivity at 9.4 K in a layered transition metal disulphide MoS_2. *Appl. Phys. Lett*. **101,** 042603 (2012).
13. Radisavljevic, B., Radenovic, A., Brivio, J., Giacometti, V. & Kis, A. Single-layer MoS_2 transistors. *Nat. Nanotechnol*. **6,** 147–150 (2011).
14. Kim, S. *et al.* High-mobility and low-power thin-film transistors based on multilayer MoS_2 crystals. *Nat. Commun*. **3,** 1011 (2012).
15. Subba Rao, G. V., Shafer, M. W., Kawarazaki, S. & Toxen, A. M. Superconductivity in alkaline earth metal and Yb intercalated group VI layered dichalcogenides. *J. Solid State Chem*. **9,** 323–329 (1974).
16. Woollam, J. A. & Somoano, R. B. Physics and chemistry of MoS_2 Intercalation compounds. *Mater. Sci. Engineer*. **31,** 289–295 (1977).
17. Shi, W. *et al.* Superconductivity series in transition metal dichalcogenides by ionic gating. *Sci. Rep*. **5,** 12534 (2015).
18. Agarwal, M. K., Patel, P. D. & Joshi, R. M. Growth conditions and structural characterization of $MoSe_xTe_{2-x}$ ($0 \leq \times \leq 2$) single crystals. *J. Mater. Sci. Lett.* **5,** 66–68 (1986).
19. Le Berre, F. *et al.* Rare-earth doping of the Mo_3Se_4 superconductor. *Physica. B* **228,** 261–271 (1996).
20. Paris, E. *et al.* Temperature dependent local atomic displacements in ammonia intercalated iron selenide superconductor, *Sci. Rep.* **6,** 27646 (2016).
21. Zhang, R. *et al.* Superconductivity in potassium-doped metallic polymorphs of MoS_2, *Nano Lett.* **16,** 629–636 (2015).
22. Tongay, S. *et al.* Thermally driven crossover from indirect toward direct bandgap in 2D semiconductors: $MoSe_2$ versus MoS_2. *Nano Lett.* **12,** 5576–5580 (2012).
23. Bougouma, M. *et al.* Growth and characterization of large, high quality $MoSe_2$ single crystals. *J. Cryst. Growth* **363,** 122–127 (2013).

Acknowledgements

This study was partly supported by Grants-in-aid (22244045, 24654105, 26105004) from MEXT, by the LEMSUPER project (JST-EU Superconductor Project) of the Japan Science and Technology Agency (JST), and by the Program for Promoting the Enhancement of Research Universities. The synchrotron XRD measurement was performed at BL10XU of Spring-8 under proposal (2015A1513).

Author Contributions

Y.K. designed this research project and supervised experiments. X.M., S.N. and L.Z. synthesized and characterized $MoSe_2$ and $(NH_3)_yM_xMoSe_2$ samples. H.T.L.N., T.K. (Osaka Univ.), N.H., Y.O., H.I. and Y.-F.L. measured the powder XRD pattern at Spring-8. X.M. and L.Z. analyzed powder XRD data. H.O. measured and analyzed the single-crystal XRD data. K.T. and T.Y. measured photoemission spectra at low temperatures. Y.K. prepared the paper with the help of X.M., H.G., R.E., T.K. (Okayama Univ.) and T.Y.

Additional Information

Supplementary information accompanies this paper at http://www.nature.com/srep

Competing financial interests: The authors declare no competing financial interests.

How to cite this article: Miao, X. *et al.* Emergence of superconductivity in $(NH_3)_yM_xMoSe_2$ (M: Li, Na and K). *Sci. Rep.* **6**, 29292; doi: 10.1038/srep29292 (2016).